




# Measurements and Calculations of Radiative Parameters for Odd-parity Levels in Nb II

Yidan Geng<sup>1</sup>, Yong Liu<sup>2</sup>, Hongfeng Zheng<sup>1</sup>, Ziqing Yu<sup>1</sup>, Ting Wang<sup>1</sup>, Pascal Quinet<sup>3,4</sup>, Bing Yan<sup>2</sup>, and Zhenwen Dai<sup>1</sup> 

<sup>1</sup> Key Laboratory of Physics and Technology for Advanced Batteries (Ministry of Education), College of Physics, Jilin University, Changchun 130012, People's Republic of China; [dai@jlu.edu.cn](mailto:dai@jlu.edu.cn)

<sup>2</sup> Institute of Atomic and Molecular Physics, Jilin University, Changchun 130012, People's Republic of China; [yanbing@jlu.edu.cn](mailto:yanbing@jlu.edu.cn)

<sup>3</sup> Physique Atomique et Astrophysique, Université de Mons, B-7000 Mons, Belgium; [pascal.quinet@umons.ac.be](mailto:pascal.quinet@umons.ac.be)

<sup>4</sup> IPNAS, Université de Liège, B-4000 Liège, Belgium

Received 2021 August 13; revised 2022 January 10; accepted 2022 January 13; published 2022 March 25

## Abstract

Experimental radiative lifetimes for 34 odd-parity levels belonging to  $4d^35p$  and  $4d^25s5s$  configurations of Nb II were measured by the time-resolved laser-induced fluorescence method. The results range from 2.2 to 11.5 ns, and 30 of them were reported for the first time, as far as we know. The theoretical radiative lifetimes for these levels were also calculated by the pseudorelativistic Hartree–Fock method including core-polarization contributions (HFR+CPOL) and the fully relativistic multiconfiguration Dirac–Hartree–Fock method, and branching fractions for these levels were also calculated by HFR+CPOL. By combining the experimental lifetimes and the calculated branching fraction values, the semiempirical transition probabilities and oscillator strengths for 389 Nb II lines were obtained.

*Unified Astronomy Thesaurus concepts:* Atomic spectroscopy (2099); Atomic physics (2063); Transition probabilities (2074); Radiative processes (2055)

*Supporting material:* machine-readable table

## 1. Introduction

Radiative parameters are of great importance in astronomy, plasma diagnostics, and analytical chemistry. Recently, Neyskens et al. (2015) used the  $N(\text{Nb})/N(\text{Zr})$  ratio in a few technetium-poor S-type stars to derive the temperature of the slow-neutron-capture process. Honda et al. (2006) reported the abundance of seven neutron-capture elements in the very metal-poor star HD 122563 for the first time, including the Nb abundance determined by two Nb II lines. Nb II lines have been observed in the solar photosphere (Nilsson et al. 2010) and many stars, such as the mild barium star HD 202109 (Yushchenko et al. 2004), the uranium-rich metal-poor star CS 31082-001 (Siqueira Mello et al. 2013), Arcturus, and V762 Cas (Karinkuzhi et al. 2018). However, there are still many Nb II lines lacking radiative parameter data. Therefore, extended measurements for radiative parameters of Nb II are more valuable to the analyses of astrophysical spectra.

The study of radiative parameters of Nb II began in 1962, when Corliss & Bozman (1962) reported experimental transition probabilities and oscillator strengths of 306 Nb II lines. Salih & Lawler (1983) determined radiative lifetimes for  $z^5G$  and  $z^3D$  levels of Nb II using the time-resolved laser-induced fluorescence method on a Nb II ion beam. The radiative lifetimes of 27 levels in Nb II were determined by the laser-induced fluorescence technique from sputtered metal vapor, and these results were combined with solar data to determine the solar abundance of Nb (Hannaford et al. 1985). Nilsson & Ivarsson (2008) used high-resolution Fourier transform spectroscopy to measure branching fractions (BFs) of 145 Nb II lines in the wavelength region 2600–4600 Å, and deduced their oscillator strengths by combining these BFs with

previously reported lifetimes. Nilsson et al. (2010) measured radiative lifetimes of 17 Nb II levels, and combined these lifetimes with BFs measured in their work to derive the transition probabilities of 107 Nb II lines relating to levels from the  $4d^35p$  configuration in the wavelength region 2240–4700 Å. Nilsson et al. (2019) reported experimental lifetimes of 13 levels in the  $4d^3(^4F)5d$  and  $4d^3(^4F)6s$  configurations at energies around  $70,000 \text{ cm}^{-1}$  by two-photon and two-step excitation schemes, and derived absolute transition probabilities of 59 lines by combining the lifetimes and BFs measured in their work.

On the theoretical side, Beck & Datta (1995) used relativistic configuration–interaction wave functions to obtain length and velocity  $f$ -values for all lower  $J=2, 3, 4$  ( $4d+5s$ )<sup>4</sup> levels connected to the  $z^4d^35p^5G^{\circ}_3$ , and  $z^3D^{\circ}_3$  levels, and derived the lifetimes of the two upper levels. Using the pseudorelativistic Hartree–Fock method including core-polarization contributions (HFR+CPOL), Nilsson et al. (2010) also reported calculated values of the lifetimes, BFs, and oscillator strengths they measured. Ruczkowski et al. (2015) calculated oscillator strengths of 251 Nb II lines using semiempirical wave functions determined via previous experimental data available, and also presented the calculated values of them by using the Cowan code package. Kurucz (2017) presented a progress report on including all the lines in the line lists and including calculations of radiative lifetimes for all the Nb II levels. Using the HFR+CPOL method, Nilsson et al. (2019) calculated the lifetimes and BFs of 13 high-lying levels between  $68,000$  and  $73,200 \text{ cm}^{-1}$  in Nb II.

Until now, experimental lifetimes of 50 Nb II levels, transition probabilities, and oscillator strengths of 477 lines that include the experimental values of Corliss & Bozman (1962) were reported. It is well known that the accuracies of the values by Corliss & Bozman (1962) are not reliable enough overall. If their results are not considered, there are 311 lines of measured transition parameters. For Nb II with a total of 353

known levels from the National Institute of Standards and Technology (NIST) database (Kramida et al. 2020), there are still many energy levels without reliable experimental radiative parameters. In this work, we measured and calculated radiative lifetimes of 34 Nb II levels, and by combining the experimental lifetimes with theoretical BFs, the semiempirical transition probabilities and oscillator strengths for 389 transitions were obtained.

## 2. Lifetime Measurements

In this work, the TR-LIF method was used to measure the radiative lifetimes of Nb II levels. The detailed description of the experimental setup used for lifetime measurements in this paper can be found in Tian et al. (2016), hence we only give a brief description of it. First of all, an ablation laser with an 8 ns pulse duration from a 532 nm Q-switched Nd:YAG laser was focused vertically on the rotated Nb target in the copper vacuum chamber with pressure of about  $10^{-4}$  Pa for generating laser-induced plasma containing singly ionized Nb. The other Nd:YAG laser was used to pump a dye laser (DCM or Rhodamine 6G dyes) to obtain a tunable excitation laser pulse. The lifetimes of most Nb II levels measured in this paper are shorter than the pulse width (8 ns) of the pump laser, therefore the pump pulse width was compressed to about 2 ns by a stimulated Brillouin scattering (SBS) compressor. A detailed description of this technique was presented by Schiemann et al. (1998), and the setup of the SBS compressor used here is the same as described in the paper by Jiang et al. (2012). The third-order harmonic of the dye laser was obtained by using two beta barium borate type-I crystals and a retarding plate, and then focused into a stimulated Raman scattering cell with H<sub>2</sub> at 11 bars to obtain the first-order Stokes component of Raman shifting as the excitation laser. Then the excitation laser was sent into the vacuum chamber perpendicular to the ablation laser about 8 mm above the Nb target. The two lasers were triggered by a digital delay generator (SRS DG535). The laser-induced fluorescence was focused into a grating monochromator by a fused silica lens and detected by a microchannel plate photomultiplier tube (PMT, Hamamatsu R3809U-58), then the signal was recorded by a 1 GHz digital oscilloscope (Keysight DSOX3102T), and passed into a personal computer.

Some possible effects may influence the lifetime results, such as the flight out of view, nonlinear response of the PMT, collisional deexcitation, radiation trapping, superradiation, and quantum beat effects. A 100 G magnetic field was applied by a pair of Helmholtz coils to remove quantum beats caused by the Earth's magnetic field. The other possible effects were minimized by optimizing the experimental conditions (Wang et al. 2018). During the measurements, we adjusted the delays in the range of 2–8  $\mu$ s with a step of 0.2 or 0.3  $\mu$ s to obtain a set of fluorescence decay curves. For each curve, more than 1000 shots were averaged to acquire a curve with good signal-to-noise ratio. In order to reduce the influence of excitation pulse width on the results, all the obtained curves were fitted to the convolution of the excitation pulse and an exponential function to evaluate the lifetime values. A fluorescence decay curve of the 50,497.841  $\text{cm}^{-1}$  level of Nb II with the convolution fit of the recorded excitation pulse and an exponential function is shown in Figure 1.

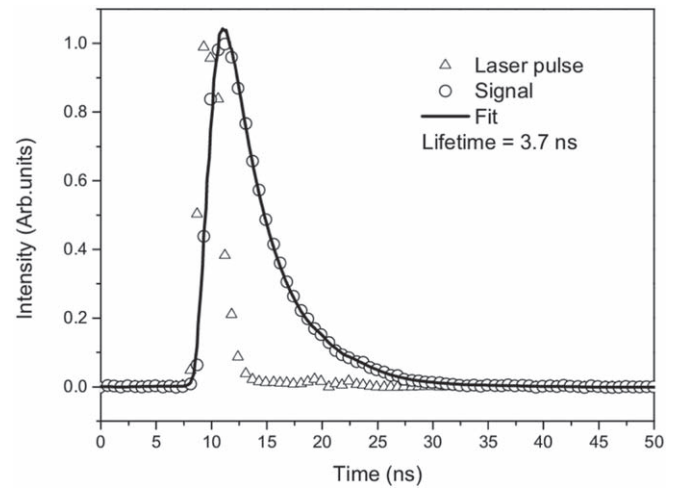


**Figure 1.** A typical fluorescence decay curve of the 50,497.841  $\text{cm}^{-1}$  level of Nb II from using an excitation pulse and an exponential function.

## 3. Theoretical Calculations

In addition to experimental lifetime measurements in Nb II, we also performed atomic structure calculations using two different and independent approaches. First, the HFR method of Cowan (1981) modified for taking core-polarization corrections into account, as described by Quinet et al. (1999, 2002), was used. Second, fully relativistic multiconfiguration Dirac–Hartree–Fock (MCDHF) calculations were performed using the Grasp2K program package (Jönsson et al. 2013).

### 3.1. HFR + CPOL Calculations

The HFR+CPOL model considered in the present work was the same as the one used in our previous works on Nb II (Nilsson et al. 2010, 2019) to which the reader is asked to refer for the details of the calculations. In summary, the physical model was based on the explicit introduction of the  $4d^4$ ,  $4d^35s$ ,  $4d^36s$ ,  $4d^35d$ ,  $4d^25s^2$ ,  $4d^25p^2$ ,  $4d^25s6s$ ,  $4d^25s5d$ ,  $4d^24f5p$ ,  $4d^25p5f$ ,  $4d^26s^2$ ,  $4d^25d^2$ ,  $4d^25d6s$ , and  $4d^25p6p$  even-parity configurations, and the  $4d^35p$ ,  $4d^36p$ ,  $4d^34f$ ,  $4d^35f$ ,  $4d^25s5p$ ,  $4d^25s6p$ ,  $4d^24f5s$ ,  $4d^24f5d$ ,  $4d^25s5f$ ,  $4d^25p6s$ ,  $4d^25p5d$ , and  $4d^26s6p$  odd-parity configurations. The core-polarization effects were estimated using the dipole polarizability corresponding to the ionic Nb IV core given in Fraga et al. (1976), i.e.,  $\alpha_d = 5.80 a_0^3$ , while the cutoff radius was chosen to be the HFR mean value of  $\langle r \rangle$  of the outermost core orbital ( $4d$ ), i.e.,  $r_c = 1.85 a_0$ . As explained in Nilsson et al. (2019), the use of these two core-polarization parameters led to calculated lifetimes systematically a few percent longer than the experimental values reported in the same paper for  $4d^36s$  and  $4d^35d$  levels. Therefore, the dipole radial integrals of the  $4d^35p$ – $4d^36s$  and  $4d^35p$ – $4d^35d$  transitions were semiempirically adjusted to fit the calculations to the experimental lifetimes. Note that without making this adjustment, i.e., using the dipole integrals not corrected for polarization effects (HFR calculation without CPOL), we obtained lifetimes about 20%–25% smaller than the experimental values. In addition, the calculated energy levels were fitted to the available experimental values reported by Ryabtsev et al. (2000), using a least-squares optimization of the radial parameters belonging to the  $4d^4$ ,  $4d^35s$ ,  $4d^36s$ ,  $4d^35d$ ,  $4d^25s^2$ ,  $4d^25p$ , and  $4d^25s5p$

configurations, according to the methodology followed by Nilsson et al. (2010). This allowed us to reproduce the experimental energy level structure with standard deviations of  $280 \text{ cm}^{-1}$  in the even parity and  $148 \text{ cm}^{-1}$  in the odd parity, i.e., with an accuracy better than 0.5% of the energy range considered.

### 3.2. MCDHF Calculations

The calculations for the radiative lifetimes of Nb II levels were carried out based on the MCDHF method (Fischer et al. 2016). Our calculation for all even and odd states was done in the extended optimal levels scheme. All the configuration state functions expansions were obtained by allowing single and double substitutions of electrons from the occupied orbitals to the virtual orbitals.

The first set of calculations was carried out using the Dirac–Hartree–Fock self-consistent field (SCF) procedure. In this step, the occupied orbitals in the reference configurations ( $4d^25s5p$ ,  $4d^35p$ ,  $4d^4$ ,  $4d^35s$  and  $4d^25s^2$ ) were optimized as spectroscopic orbitals. The  $4d$ ,  $5s$ , and  $5p$  orbitals are the valence orbitals and the others are the core orbitals. All the occupied orbitals were optimized, but kept frozen in the subsequent steps. In the following SCF calculations, the core–valence correlation and the valence–valence correlation were considered. To monitor the convergence of the calculated energies, the active spaces were enlarged layer by layer up to  $n_{\text{max}} = 9$  and  $l_{\text{max}} = 5$  for the virtual orbitals, and only the last-added virtual orbitals were optimized in each newly added layer. The SCF calculations were followed by relativistic configuration–interaction calculations, including the Breit interaction and leading QED effects (vacuum polarization and self-energy). For electric dipole transitions, there are two forms of the transition operator, the length (Babushkin) and the velocity (Coulomb) forms. Since the length form is more sensitive to the exterior of the wave functions, we only list the relevant results under length form in the present work. Furthermore, the lifetime  $\tau_i$  of the upper state  $i$  can be determined by  $\tau_i = 1/\sum_j A_{ij}$ , where  $A_{ij}$  is the transition probabilities, and  $j$  represents all the states of dipole-allowed transition below the state  $i$ .

## 4. Results and Discussion

The experimental and theoretical radiative lifetimes measured in this work for 34 Nb II levels are listed in Table 1. The assignments and energies of these levels are from the Atomic Spectra Database at NIST (Kramida et al. 2020). The final uncertainties of the lifetime values consist of systematic errors and statistical scattering errors from different recordings. For each level, a set of curves recorded under different conditions would give their own lifetime results. The standard deviation of these values was employed as the statistical uncertainty. Moreover, we can get two lifetime values for a curve using two excitation pulses recorded before and after the curve registration, respectively, and their difference was used to evaluate the systematic error. It can be seen that most of the uncertainties of our measured results are less than 10%. The semiempirical superposition-of-configuration calculations for these levels by Kurucz (2017) are also listed in Table 1 for comparison. For the levels 34,886.354, 43,290.338, and  $43,887.078 \text{ cm}^{-1}$ , our results are in good agreement with those reported by Salih & Lawler (1983), Hannaford et al.

(1985), and Nilsson et al. (2010) within  $\pm 10\%$ , with ours as the reference ((ours – theirs)/ours). For the level  $44,066.665 \text{ cm}^{-1}$ , our result  $6.4 \pm 0.3 \text{ ns}$  is in line with the value  $6.4 \pm 0.5 \text{ ns}$  presented by Nilsson et al. (2010), but it has a slightly larger difference compared with the value  $5.3 \pm 0.3 \text{ ns}$  reported by Hannaford et al. (1985).

Our HFR+CPOL and MCDHF theoretical lifetimes are also given in Table 1. The HFR+CPOL results show an overall good agreement with the measured data, the mean ratio  $\tau_{\text{HFR+CPOL}}/\tau_{\text{EXP}}$  being found to be equal to  $1.11 \pm 0.27$ , where the uncertainty corresponds to the standard deviation of the mean. For the MCDHF method, most of the theoretical lifetimes are in agreement with the corresponding experimental values, excluding the calculated lifetime of the level  $46,343.093 \text{ cm}^{-1}$  that was calculated to be 2.6 ns, which is about a factor of 4 lower than the experimental value of 10.0 ns, and there are differences of a factor of 2 between the experimental and theoretical lifetimes for the levels at  $48,627.192$ ,  $49,186.838$ ,  $49,733.457$ , and  $50,447.348 \text{ cm}^{-1}$ . In any case, the experimental values must be considered as the reference values. At the same time, we plot the deviation between the experimental and calculated lifetimes in Figure 2 to compare the results between the two different theoretical methods more clearly. It is seen from Figure 2 that except for some levels with larger differences, the deviations of the two calculation methods are roughly similar. However, it is interesting to note that the largest differences between the two theoretical approaches correspond to very strongly mixed energy levels. For example, for the level at  $46,343.093 \text{ cm}^{-1}$ , for which the HFR+CPOL and MCDHF lifetimes differ by a factor of 5, the first two components in Russell–Saunders ( $LS$ ) coupling were found to be of comparable magnitude ( $\sim 30\% 4d^3(^2D)5p^3P_2 + 30\% 4d^3(^2P)5p^3P_2$ ) according to our calculations. This leads to a high sensitivity of the lifetime calculation to any slight variation in the eigenvector composition. Since the deviation between the MCDHF and experimental lifetimes shows a slightly larger dispersion ( $\tau_{\text{MCDHF}}/\tau_{\text{EXP}} = 1.11 \pm 0.39$ ) than that obtained with the HFR+CPOL results on the one hand, and since the energy levels computed in the latter approach were semiempirically fitted to reproduce, at best, the experimental level structure on the other hand, we chose to rely on the HFR+CPOL calculations to determine the radiative parameters corresponding to Nb II transitions.

BFs, transition probabilities ( $gA$ ), and oscillator strengths ( $\log gf$ ) obtained in the present work for highly excited levels of Nb II are reported in Table 2. The BF values given in this table were obtained using our HFR+CPOL model and were combined with the experimental lifetimes to deduce the  $gA$  and  $gf$  values for all transitions with  $\text{BF} > 0.01$  depopulating the 34 energy levels considered in our work. This represents 389 spectral lines covering the wavelength range between 205 and 530 nm. The uncertainties of the transition probabilities and oscillator strengths were estimated using the same criteria as those used in our previous works on Ir I (Zhou et al. 2018), Ba I (Wang et al. 2019), and Rh I (Li et al. 2021), in which a rather regular trend of deviations between the calculated HFR+CPOL BFs and available experimental measurements was noticed, so that the average uncertainties on computed BF values appeared to be systematically about 10%–20% for  $0.8 < \text{BF} < 1.0$ , 20%–30% for  $0.6 < \text{BF} < 0.8$ , 30%–40% for  $0.4 < \text{BF} < 0.6$ , 40%–50% for  $0.2 < \text{BF} < 0.4$ , and 50%–100% for  $0.0 < \text{BF} < 0.2$ .

**Table 1**  
Measured Lifetimes for Nb II Levels and Comparison with Previous Results

Upper Level <sup>a</sup>		Lower Level <sup>a</sup>		$\lambda_{\text{Exc}}$ (nm)	$\lambda_{\text{Obs}}$ (nm)	Lifetime (ns)					
Assignment	Energy (cm <sup>-1</sup> )	Assignment	Energy (cm <sup>-1</sup> )			This Work			Previous		
				Exp.	HFR	MCDHF	Exp.	HFR <sup>d</sup>	Kurucz <sup>e</sup>		
$4d^3(^4F)5p^3D^{\circ}_1$	34,886.354	$4d^3(^4F)5s^5F_2$	2629.132	310.008	349	5.6(3)	5.9	6.3	5.5(3) <sup>b</sup> , 5.7(3) <sup>c</sup> , 5.6(3) <sup>d</sup>	5.1, 5.9	4.5
$4d^3(^4P)5p^5D^{\circ}_2$	43,290.338	$4d^4^5D_1$	158.984	231.850	424	7.5(5)	7.3	7.9	7.5(4) <sup>d</sup>	6.9, 7.3	5.4
$4d^3(^4P)5p^5P^{\circ}_1$	43,449.991	$4d^4^5D_1$	158.984	230.995	232	2.7(3)	2.8	2.8			1.9
$4d^3(^4P)5p^5D^{\circ}_3$	43,887.078	$4d^4^5D_2$	438.361	230.156	344	5.9(4)	6.3	6.6	5.7(5) <sup>d</sup>	5.9, 6.3	5.0
$4d^3(^4P)5p^5D^{\circ}_1$	44,066.665	$4d^4^5D_2$	438.361	229.209	396	6.4(3)	6.7	6.7	5.3(3) <sup>c</sup> , 6.4(5) <sup>d</sup>	5.8, 6.7	5.5
$4d^3(^2G)5p^1F^{\circ}_3$	44,638.752	$4d^4^5D_3$	801.326	228.116	238	3.9(2)	3.7	2.8			3.3
$4d^3(^2G)5p^1H^{\circ}_3$	45,342.236	$4d^4^3H_6$	10,186.390	284.448	357	5.1(2)	6.5	6.8			5.2
$4d^3(^2G)5p^3F^{\circ}_4$	45,621.897	$4d^4^3G_4$	10,604.229	285.570	313	3.4(4)	4.0	3.9			3.0
$4d^3(^2G)5p^3G^{\circ}_4$	46,295.605	$4d^4^3G_5$	10,918.474	282.668	307	2.5(3)	3.4	4.5			2.5
$4d^3(^2D)5p^3P^{\circ}_2$	46,343.093	$4d^3(^4F)5s^5F_2$	2629.132	228.760	286	10.0(8)	13.5	2.6			9.4
$4d^3(^2P)5p^3S^{\circ}_1$	46,358.910	$4d^4^5D_0$	0	215.708	245	3.6(3)	3.3	3.8			2.8
$4d^2(^3F)5s5p(^3P^{\circ})^5G^{\circ}_3$	46,949.540	$4d^4^5D_2$	438.361	215.002	230	11.5(11)	19.2	13.2			13.2
$4d^3(^4P)5p^5S^{\circ}_2$	47,072.965	$4d^4^5D_1$	158.984	213.156	227	5.8(5)	6.6	6.6			5.6
$4d^3(^2D)5p^3F^{\circ}_2$	47,755.756	$4d^4^5D_2$	438.361	211.339	224	4.5(4)	6.6	5.9			4.7
$4d^3(^2D)5p^3F^{\circ}_3$	48,077.679	$4d^4^5D_2$	438.361	209.911	222	4.9(5)	7.0	6.1			5.1
$4d^3(^2H)5p^3I^{\circ}_5$	48,130.475	$4d^4^5D_4$	1224.823	213.194	224	6.2(10)	5.2	6.1			4.2
$4d^3(^2G)5p^1G^{\circ}_4$	48,253.418	$4d^4^5D_4$	1224.823	212.637	224	6.6(6)	7.2	4.7			5.4
$4d^3(^2D)5p^3D^{\circ}_1$	48,520.374	$4d^4^3D_1$	13,118.528	282.471	319	2.2(5)	2.7	2.7			2.0
$4d^3(^2D)5p^3F^{\circ}_4$	48,627.192	$4d^4^5D_4$	1224.823	210.960	222	4.2(5)	6.6	9.2			4.5
$4d^2(^3F)5s5p(^3P^{\circ})^5F^{\circ}_1$	49,186.838	$4d^3(^4F)5s^5F_1$	2356.816	213.538	275	7.5(10)	2.8	2.5			1.9
$4d^3(^4P)5p^3D^{\circ}_2$	49,245.468	$4d^3(^4F)5s^5F_1$	2356.816	213.271	325	3.8(3)	4.1	4.5			3.2
$4d^3(^2D)5p^1P^{\circ}_1$	49,687.712	$4d^3(^4F)5s^5F_1$	2356.816	211.278	256	2.6(3)	4.0	2.6			2.8
$4d^3(^4P)5p^3D^{\circ}_1$	49,733.457	$4d^3(^4F)5s^5F_1$	2356.816	211.074	237	2.5(3)	2.5	5.6			2.0
$4d^3(^4P)5p^3D^{\circ}_3$	49,759.194	$4d^3(^4F)5s^5F_2$	2629.132	212.179	257	2.8(3)	3.6	3.6			2.5
$4d^3(^2D)5p^3D^{\circ}_3$	49,864.296	$4d^3(^4F)5s^5F_2$	2629.132	211.707	331	2.9(3)	2.4	2.6			2.3
$4d^2(^3F)5s5p(^3P^{\circ})^5F^{\circ}_3$	50,068.799	$4d^3(^4F)5s^5F_3$	3029.629	212.589	255	2.9(3)	2.8	2.5			1.9
$4d^3(^2P)5p^3P^{\circ}_2$	50,447.348	$4d^3(^4F)5s^5F_2$	2629.132	209.125	346	5.8(9)	2.9	3.9			2.5
$4d^3(^2D)5p^3P^{\circ}_1$	50,474.935	$4d^3(^4F)5s^5F_2$	2629.132	209.005	233	3.6(3)	3.2	3.9			2.7
$4d^3(^2H)5p^3G^{\circ}_5$	50,497.841	$4d^3(^4F)5s^5F_4$	3542.561	212.969	272	3.7(2)	3.9	3.5			2.8
$4d^2(^3F)5s5p(^3P^{\circ})^5F^{\circ}_4$	50,552.237	$4d^3(^4F)5s^5F_3$	3029.629	210.426	397	2.7(2)	2.9	2.6			2.1
$4d^3(^2H)5p^3G^{\circ}_3$	50,585.228	$4d^3(^4F)5s^5F_3$	3029.629	210.280	381	3.1(3)	3.7	4.3			2.1
$4d^3(^2H)5p^3G^{\circ}_4$	50,851.663	$4d^3(^4F)5s^5F_4$	3542.561	211.376	392	3.7(5)	3.8	4.3			2.6
$4d^2(^3F)5s5p(^3P^{\circ})^5F^{\circ}_5$	51,537.014	$4d^3(^4F)5s^5F_4$	3542.561	208.357	382	2.5(2)	2.8	3.0			1.9
$4d^2(^3F)5s5p(^3P^{\circ})^3F^{\circ}_4$	52,279.590	$4d^3(^4F)5s^5F_5$	4146.037	207.755	196	2.2(2)	2.3	2.2			1.7

**Notes.**<sup>a</sup> Kramida et al. (2020).<sup>b</sup> Salih & Lawler (1983).<sup>c</sup> Hannaford et al. (1985).<sup>d</sup> Nilsson et al. (2010).<sup>e</sup> Kurucz (2017).



**Table 2**  
BFs, Transition Probabilities, and Oscillator Strengths Obtained in the Present Work for Highly Excited Levels of Nb II, and a Comparison with Previous Results (Sample)

Upper Level <sup>a</sup>		Lower Level <sup>a</sup>		$\lambda_{\text{air}}$ (nm)	BF <sup>b</sup>	$gA$ ( $10^6 \text{ s}^{-1}$ )		Log( $gf$ )		
Assign.	$E$ ( $\text{cm}^{-1}$ ) Lifetime (ns)	Assign.	$E$ ( $\text{cm}^{-1}$ )			This Work <sup>c</sup>	Previous	This Work <sup>c</sup>	Previous	
								Exp.	Calc. <sup>f</sup>	
$4d^3(^4F)5p\ ^3D^{\circ}_1$	34,886.354 $\tau = 5.6(3)$	$4d^4\ ^5D_0$	0.000	286.561	0.098	52.6 (E)	55.0 <sup>d</sup> , 53.8 <sup>e</sup>	-1.19 (E)	-1.17 <sup>d</sup> , -1.179 <sup>e</sup> , -1.192 <sup>f</sup>	-1.122
		$4d^4\ ^5D_1$	158.984	287.873	0.033	17.8 (E)	37.0 <sup>d</sup>	-1.66 (E)	-1.34 <sup>d</sup>	
		$4d^3(^4F)5s\ ^5F_1$	2356.816	307.324	0.091	48.8 (E)	47.0 <sup>d</sup> , 45.8 <sup>e</sup>	-1.16 (E)	-1.17 <sup>d</sup> , -1.188 <sup>e</sup> , -1.202 <sup>f</sup>	-0.984
		$4d^3(^4F)5s\ ^5F_2$	2629.132	309.918	0.161	86.4 (D)	68.0 <sup>d</sup> , 82.2 <sup>e</sup>	-0.90 (D)	-1.01 <sup>d</sup> , -0.926 <sup>e</sup> , -0.966 <sup>f</sup>	-0.825
		$4d^4\ ^3P_0$	5562.241	340.918	0.136	73.0 (E)	96.0 <sup>d</sup> 77.4 <sup>e</sup>	-0.90 (E)	-0.77 <sup>d</sup> , -0.870 <sup>e</sup> , -0.883 <sup>f</sup>	-0.878
		$4d^4\ ^3P_1$	6192.310	348.404	0.088	47.3 (E)	54.0 <sup>d</sup> 47.4 <sup>e</sup>	-1.06 (E)	-1.01 <sup>d</sup> , -1.064 <sup>e</sup> , -1.063 <sup>f</sup>	-1.053
		$4d^4\ ^3P_2$	7261.324	361.888	0.023	12.3 (E)		-1.62 (E)		
		$4d^4\ ^3F_2$	7505.765	365.118	0.308	165 (D)	230 <sup>d</sup> 164 <sup>e</sup>	-0.48 (D)	-0.35 <sup>d</sup> , -0.483 <sup>e</sup> , -0.510 <sup>f</sup>	-0.490
		$4d^4\ ^3D_2$	12,805.965	452.764	0.018	9.80 (E)	15.0 <sup>d</sup> 16.6 <sup>e</sup>	-1.52 (E)	-1.35 <sup>d</sup> , -1.293 <sup>e</sup> , -1.289 <sup>f</sup>	-1.559
		$4d^3(^4F)5s^3F_2$	13,479.460	467.008	0.029	15.8 (E)		-1.29 (E)		

**Notes.**<sup>a</sup> Kramida et al. (2020).<sup>b</sup> Branching fractions calculated using the HFR+CPOL method.<sup>c</sup>  $gA$  and  $\log gf$  values obtained in this work were deduced from the combination of HFR+CPOL BFs with experimental lifetimes. The estimated uncertainties are given in parentheses. They are indicated by the same code letter as the one used in the NIST database (Kramida et al. 2020), i.e., B ( $\leq 10\%$ ), C+ ( $\leq 18\%$ ), C ( $\leq 25\%$ ), D+ ( $\leq 40\%$ ), D ( $\leq 50\%$ ) and E ( $> 50\%$ ) (see text).<sup>d</sup> Corliss & Bozman (1962).<sup>e</sup> Nilsson & Ivarsson (2008).<sup>f</sup> Ruczkowski et al. (2015).<sup>g</sup> Nilsson et al. (2010).<sup>h</sup> Hannaford et al. (1985).

(This table is available in its entirety in machine-readable form.)

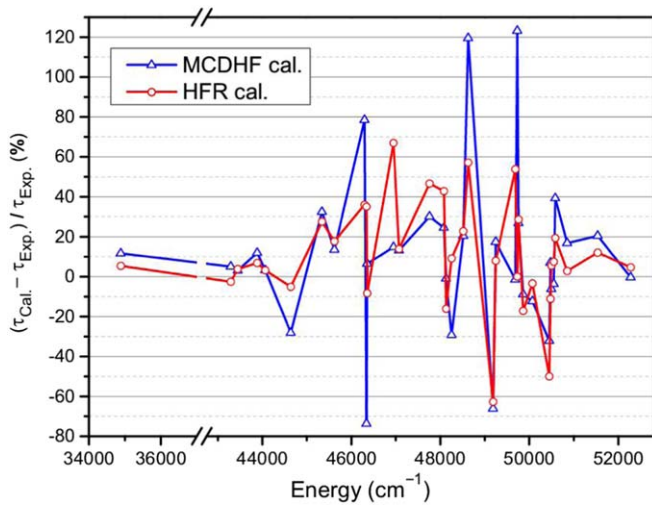


**Figure 2.** Comparison of deviation between theoretical (MCDHF and HFR) and experimental lifetimes.

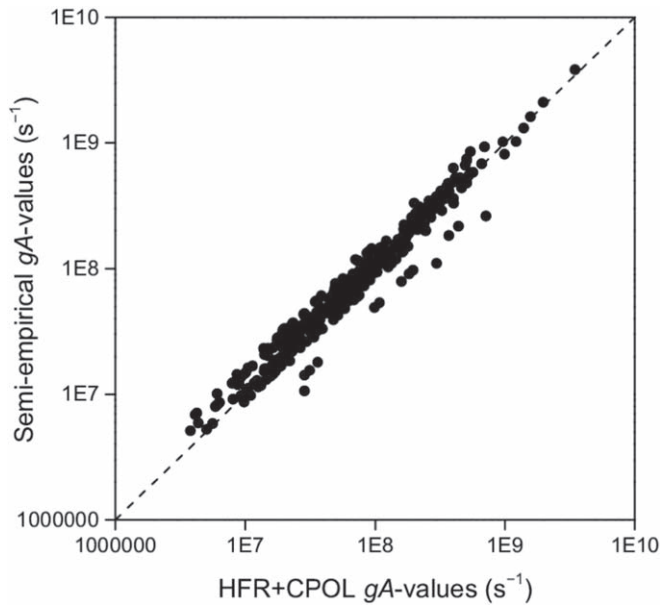


**Figure 3.** Comparison between the semiempirical and theoretical HFR+CPOL weighted transition probabilities ( $gA$ ) obtained in the present work for Nb II spectral lines.

This increasing uncertainty for transitions with smaller BFs obviously stems from the fact that, for these weak lines, the energy levels are highly mixed (and thus very sensitive to slight variations of the compositions in the calculations) or the line strengths are affected by annihilation effects (see, e.g., Cowan 1981). As a consequence, the same letter coding as the one used in these latter papers, inspired by the one usually employed in the NIST database (Kramida et al. 2020), was also used here, i.e., B (= 10%), C (= 25%), D+ (= 40%), D (= 50%), and E (> 50%). The uncertainties given in Table 2 were obtained by combining in quadrature the uncertainties affecting our HFR+CPOL BF values and those affecting our experimental lifetimes.

When comparing with the few available data for the same transitions (also given in Table 2), we can note a very good agreement (in general within a few percent) between our

oscillator strengths and the experimental values published by Hannaford et al. (1985), Nilsson & Ivarsson (2008), Nilsson et al. (2010) and the semiempirical data obtained by Ruczkowski et al. (2015), while much larger discrepancies with the  $gA$  and  $gf$  values tabulated by Corliss & Bozman (1962) are observed but it is now well established that the latter results show very high inaccuracies in many cases. Finally, it is worth noting that our semiempirical  $gf$  and  $gA$  values deviate from the purely theoretical HFR+CPOL results by only 22% on average, as illustrated in Figure 3, thus allowing us to conclude that the new radiative parameters presented in this work constitute a much more realistic and reliable data set than the one published by Corliss & Bozman (1962) for Nb II transitions.

This work was supported by the National Natural Science Foundation of China (grant Nos. U1832114 and 11874177). Y. L. would like to thank Dr. Chengbin Li from Wuhan Institute of Physics and Mathematics, Chinese Academy of Sciences, for help and guidance in computations. Pascal Quinet is Research Director of the Belgian F.R.S.-FNRS and he wishes to thank this organization for its financial support.

### ORCID iDs

Zhenwen Dai  <https://orcid.org/0000-0002-9040-2315>

### References

- Beck, D. R., & Datta, D. 1995, *PhRvA*, **52**, 2436
- Corliss, C. H., & Bozman, W. R. 1962, Experimental Transition Probabilities for Spectral Lines of Seventy Elements (Washington, DC: National Bureau of Standards), 247
- Cowan, R. D. 1981, The Theory of Atomic Structure and Spectra (Berkeley, CA: Univ. California Press)
- Fischer, C. F., Godefroid, M., Brage, T., et al. 2016, *JPhB*, **49**, 182004
- Fraga, S., Karwowski, J., & Saxena, K. M. S. 1976, Handbook of Atomic Data (Amsterdam: Elsevier)
- Hannaford, P., Lowe, R. M., Biémont, E., & Grevesse, N. 1985, *A&A*, **143**, 447
- Honda, S., Aoki, W., Ishimaru, Y., Wanajo, S., & Ryan, S. G. 2006, *ApJ*, **643**, 1180
- Jiang, L. Y., Wang, Q., Feng, Y. Y., et al. 2012, *EPJD*, **66**, 176
- Jönsson, P., Gaigalas, G., Bieroń, J., Fischer, C. F., & Grant, I. P. 2013, *Comput. Phys. Commun.*, **184**, 2197
- Karinkuzhi, D., Van Eck, S., Jorissen, A., et al. 2018, *A&A*, **618**, A32
- Kramida, A., Ralchenko, Yu., Reader, J. & NIST ASD Team 2020, NIST Atomic Spectra Database (v5.8) (Gaithersburg, MD: National Institute of Standards and Technology), <https://physics.nist.gov/asd>
- Kurucz, R. L. 2017, Kurucz/Atoms, <https://kurucz.harvard.edu/atoms.html>
- Li, Y., Geng, Y., Liu, M., et al. 2021, *MNRAS*, **503**, 5085
- Neyskens, P., Van Eck, S., Jorissen, A., et al. 2015, *Natur*, **517**, 174
- Nilsson, H., Engström, L., Lundberg, H., et al. 2019, *A&A*, **627**, A102
- Nilsson, H., Hartman, H., Engström, L., et al. 2010, *A&A*, **511**, A16
- Nilsson, H., & Ivarsson, S. 2008, *A&A*, **492**, 609
- Quinet, P., Palmeri, P., Biémont, E., et al. 1999, *MNRAS*, **307**, 934
- Quinet, P., Palmeri, P., Biémont, E., et al. 2002, *J. Alloys Compd.*, **344**, 255
- Ruczkowski, J., Bouazza, S., Elantkowska, M., & Dembczyński, J. 2015, *JQSRT*, **155**, 1
- Ryabtsev, A. N., Churilov, S. S., & Litzén, U. 2000, *PhyS*, **62**, 368
- Salih, S., & Lawler, J. E. 1983, *PhRvA*, **28**, 3653
- Schiemann, S., Hogervorst, W., & Ubachs, W. 1998, *IJQE*, **34**, 407
- Siqueira Mello, C., Jr., Spite, M., Barbuy, B., et al. 2013, *A&A*, **550**, A122
- Tian, Y. S., Wang, X. H., Yu, Q., et al. 2016, *MNRAS*, **457**, 1393
- Wang, Q., Gamrath, S., Palmeri, P., et al. 2019, *JQSRT*, **225**, 35
- Wang, X. H., Quinet, P., Li, Q., et al. 2018, *JQSRT*, **212**, 112
- Yushchenko, A. V., Gopka, V. F., Kim, C., et al. 2004, *A&A*, **413**, 1105
- Zhou, L. N., Gamrath, S., Palmeri, P., et al. 2018, *ApJS*, **238**, 3